Combined Effect of Surface Nano-Topography and Delivery of Therapeutics on the Adhesion of Tumor Cells on Porous Silicon Substrates

S. De Vitis, M.L. Coluccio, G. Strumbo, N. Malara, F.P. Fanizzi, S.A. De Pascali, G. Perozziello, P. Candeloro, E. Di Fabrizio, F. Gentile

PII: S0167-9317(16)30076-4
DOI: doi: 10.1016/j.mee.2016.02.033
Reference: MEE 10145

To appear in:

Received date: 20 October 2015
Revised date: 14 February 2016
Accepted date: 20 February 2016

Please cite this article as: S. De Vitis, M.L. Coluccio, G. Strumbo, N. Malara, F.P. Fanizzi, S.A. De Pascali, G. Perozziello, P. Candeloro, E. Di Fabrizio, F. Gentile, Combined Effect of Surface Nano-Topography and Delivery of Therapeutics on the Adhesion of Tumor Cells on Porous Silicon Substrates, (2016), doi: 10.1016/j.mee.2016.02.033

Combined Effect of Surface Nano-Topography and Delivery of Therapeutics on the Adhesion of Tumor Cells on Porous Silicon Substrates

De Vitis S[a], Coluccio ML[a], Strumbo G[a], Malara N[a], Fanizzi FP[b], De Pascali SA[b], Perozziello G[a], Candeloro P[a], Di Fabrizio E[b], Gentile F[a,c,*]

[a] Department of Experimental and Clinical Medicine, University Magna Graecia, Catanzaro, Italy

[b] Department of Environmental Biological Sciences and Technologies, University of Salento, Lecce, Italy

[c] King Abdullah University of Science and Technology, Thuwal, Saudi Arabia

[d] Department of Electrical Engineering and Information Technology, University Federico II, Naples, Italy

[*] Corresponding author: gentile@unicz.it, francesco.gentile2@unina.it

Abstract

Porous silicon is a nano material in which pores with different sizes, densities and depths are infiltrated in conventional silicon imparting it augmented properties including biodegradability, biocompatibility, photoluminescence. Here, we realized porous silicon substrates in which the pore size and the fractal dimension were varied over a significant range. We loaded the described substrates with a $PtCl(O,O'-acac)(DMSO)$ antitumor drug and determined its release profile as a function of pore size over time up to 15 days. We observed that the efficacy of delivery augments with the pore size moving from small ($\sim 8\ nm$, efficiency of delivery ~ 0.2) to large ($\sim 55\ nm$, efficiency of delivery ~ 0.7). Then, we verified the adhesion of MCF-7 breast cancer cells on the described substrates with and without the administration of the antitumor drug. This permitted to decouple and understand the coincidental effects of nano-topography and a controlled dosage of drugs on cell adhesion and growth. While large pore sizes guarantee elevated drug dosages, large fractal dimensions boost cell adhesion on a surface. For the particular case of tumor cells and the delivery of an anti-tumor drug, substrates with a small fractal dimension and large pore size hamper cell growth. The competition between nano-topography and a controlled dosage of drugs may either accelerate or block the adhesion of cells on a nanostructured surface, for applications in tissue engineering, regenerative medicine, personalized lab-on-a-chips, and the rational design of implantable drug delivery systems.

Keywords: Porous Silicon, Nano-Topography, Drug Delivery, Anti-tumour drug, Cell Adhesion

1 Introduction

Porous silicon (PSi) is a nano-material in which conventional silicon is modified through electrochemical procedures to contain a layer of pores within its structure[1, 2]. The artificially introduced network of pores may vary in size and shape to a large extent and the distribution of these in the porous matrix can be finely adjusted on changing few parameters of the fabrication process, including etching time, current intensity, active etchant concentration, temperature of the process[1, 2]. Depending on pore size, shape and density the micro-structure of PSi reveals an increased surface to volume ratio, up to 500 folds, and this increment is responsible for a number of properties of PSi including, but not limited to, biodegradability under physiological conditions[3], biocompatibility[4, 5], hydrophobicity[1], photoluminescence[6]. Taken together, these and other not described properties render PSi a biomaterial, that is, a substance which can be engineered to take a form which, alone or as part of a complex system, may be used to direct the course of any therapeutic or diagnostic procedure. Porous silicon and its more sophisticated evolutions have been employed for time[7, 8] and space[9] resolved drug delivery systems, for the separation of the low molecular weight content of a mixture for spectroscopic and spectrometric analysis[10-14], for the sequencing of DNA[15] or nanoparticles[16]. In few cases, porous silicon substrates with a fixed[2] or smoothly variable pore size[17] were used to verify the adhesive behavior of cells as a function of surface topography. Recalling that, according to the IUPAC definition[3], surfaces with a pore size smaller than $2\ nm$, comprised between 2 and $50\ nm$, and larger than $50\ nm$, are categorized as micro-porous (MiP), meso-porous (MeP) and macro-porous (MaP) silicon, respectively, results presented in[2, 17] indicate that nano-scale surface topography with feature sizes in the low MeP regime accelerate cell growth and adhesion. In line with the presented results, in [18] it has been demonstrated that porous silicon chips (with a small pore size ranging from $8\ nm$ to $75\ nm$ and large fractal dimensions up to $D_f \sim 2.8\ nm$) may boost the assembly of neuroblastoma N2A cells into highly clustered networks in comparison to un-etched silicon. Fractal dimension is a non-conventional parameter that describes a surface over multiple scales[1]. It provides in a sole number a measure of the complexity of a pattern, given as the amount of change of the details in a pattern to its scale. Fractal dimension may describe more efficaciously than roughness the topography of pattern. A technical description of fractals and the significance of fractal dimension may be found in references[1, 2] and in the Materials and Methods.

Here, we demonstrate the fabrication of MeP and MaP Si substrates in which the average pore size varies in the $10-60\ nm$ range, and the fractal dimension transitions from $D_f \sim 2.8$ for the substrates in the low MeP regime, to $D_f \sim 2.6$ for the intermediate MeP regime, to $D_f \sim 2.7$ for the MaP structures, where the substrates are here reported in order of pore size. The described substrates were loaded with a $PtCl(O,O'-acac)(DMSO)$ antitumor drug ($MW \sim 408$) and its secretory profile was determined through different pore sizes. This permitted to verify the rate of drug delivery and the duration of therapeutic efficacy over time up to 15 days. The described devices were used as substrates for culturing MCF-7 breast cancer cells. Cell adhesion was verified on the described substrates with and without the administration of the antitumor drug. This permitted to untangle how the competition between nano-topography and a controlled dosage of drugs may either accelerate or block the adhesion of cells on a nanostructured surface, for applications in tissue engineering, regenerative medicine, personalized lab-on-a-chips, and the rational design of implantable drug delivery systems.

2 Materials and Methods

2.1 Fabrication of the porous surfaces. Porous silicon substrates were obtained by anodization of silicon following the methods reported in [2, 18] and here briefly recapitulated. We used p-type, (100) silicon wafers with a low $0.05-0.10\ \Omega/cm$ resistivity as a substrate. The samples were cleaned with acetone and ethanol to remove possible contaminants. We obtained different pore morphologies on changing the parameters of the process. For substrates in the low MeP regime (average pore size $< 15\ nm$), we used a combination of HF, D.I. water, and ethanol in the electrolyte where the components of the solution stand in the $(1:1:2,\ v/v/v)$ ratios. In this case, the current density was adjusted as $20\ mA/cm^2$ and maintained for 5 min at $25°C$. Differently, for substrates in the high MeP regime (average pore size $> 15\ nm$) we used a mixture of HF, D.I. water, and methanol for the electrolyte in which these parts stand in a proportion of $(5:3:2,\ v/v/v)$. For this configuration, the current density was adjusted as $4\ mA/cm^2$ for 5 min at $25°C$. Finally, MaP silicon samples were fabricated applying a current density of $4\ mA/cm^2$ for 4 min at $25°C$ to an electrolyte mixture of HF, D.I. water and DMF $(9:1:115,\ v/v/v)$. After electrochemical etching, the samples were rinsed in D.I. water,

ethanol, and pentane with steps of 4 min. The porous substrate were baked at $200°C$ for 6 hours to assure hydrophilicity.

2.2 Atomic Force Microscopy characterization of the samples. The structure of the porous substrates was quantitatively determined using Atomic Force Microscopy (combined Raman-AFM Witec alpha300 RA). The samples were imaged using an intermittent, non-contact modality over a sampling area of $500 \times 500\ nm^2$ at room temperature. Ultra-sharp silicon tips (ACLA-SS, AppNano) with a curvature radius at the tip less than 5 nm were used. The final images were averaged over multiple measurements (at least four), each of them performed at a scanning rate of $1\ Hz$. The images (1024×1024 points in size) were corrected using the Witec Project 2.10® software. The characteristic power spectrum (PS) and then the fractal dimension were derived for all the substrates (Figure 2).

2.3 SEM characterization of the samples. The porous samples were verified using SEM. A Dual Beam (SEM-FIB) FEI Nova 600 NanoLab system was used for all the acquisitions, in which the beam energy was adjusted to $15\ keV$ and the electron current accordingly to $0.14\ nA$. The pores, where the average pore size is in some cases comprised in the low nano-meter range, were resolved using a specific imaging modality, named mode 2, whereby sample can be magnified over 2.5 million times.

2.4 Fourier analysis and fractal dimension of the substrates. Fractals are entities that are too irregular to be described by conventional geometry. They display the following properties[1]: (fractals) (i) have a fine structure, that is, they reveal details on arbitrarily small scales; (ii) can be generated by short algorithms (perhaps recursively); (iii) exhibit a fractal dimension D_f strictly greater than the classical topological dimension: that is to say, the fractal dimension of a surface is generally greater than 2. In addition to this, self-affine fractal surfaces are hierarchical, that is, they are generated by the repetition of the same structure over multiple scales. Here, we used the methods described in [19, 20], to analyse the AMF images of the samples (Figure 2) and extract from each image the power spectrum $C(q)$ which reads

$$C(q) = \frac{H}{2\pi}\left(\frac{h_o}{q_o}\right)^2 \left(\frac{q}{q_o}\right)^{-2(H+1)}, q > q_o \quad (1)$$

where q is the wave-number, λ is the wavelength (and notice that $q = 2\pi/\lambda$), q_o is the lower cut-off wavenumber and thus $\lambda_o = 2\pi/q_o$, and $h_o = \sqrt{2}\,Rrms$. Moreover, we assume that the considered fractal surface is self-affine. In Equation (1), H is the Hurst coefficient. In a diagram in which we

display the logarithm of $C(q)$ against the logarithm of q, $C(q)$ takes the form of a line with a slope β for $q > q_o$. In this dimensionality range, $\beta = 2(H + 1)$ and the fractal dimension $D_f = (8 - \beta)/2$.

2.5 Determining the drug release profiles. $PtCl(O, O' - acac)(DMSO)$ is a new platinum(II) complex containing acetylacetonate ($acac$) in the coordination sphere of the metal, with the ability to induce cell death in human cervical carcinoma HeLa cells, in human breast cancer cells MCF-7 and in primary cultured human breast epithelial cells[21]. Here, we prepared 30 μM solutions of $PtCl(O, O' - acac)(DMSO)$ in D.I. water. We incubated the porous samples with the described solutions for 60 h. Then, we verified the release of molecules over time up to 15 days using UV-VIS spectroscopy techniques (spectrophotometer UV/Vis - LAMBDA 25 UV/Vis PerkinElmer), after standard calibration procedures of the samples.

2.6 Culturing cells on the porous substrates. We used here MCF-7 breast carcinoma cells. Cells were supplemented with Dulbecco's modified eagle's medium (DMEM, Euroclone) with the addition of 10% heat-inactivated fetal bovine serum (Euroclone), streptomycin (0.2 $mg\ ml^{-1}$) and penicillin (200 $IU\ ml^{-1}$). They were cultured at 37 °C with a controlled 5% CO_2 in an incubator on a petri dish. At 90% confluence, cell culture medium was replaced with a solution of 0.25% Trypsin-0.53mM EDTA (Euroclone) for 5 minutes. Trypsin was first deactivated and then removed by centrifugation at 1300 rpm for 5 minutes at a low 18°C T. The samples (with and without the exposition to drugs) were sterilized and placed into individual cell of a multi well plate (Corning Incorporated). Then, they were washed with a phosphate-buffered saline solution (PBS, Invitrogen). Cells were cultured on the substrates in a complete cell culture medium and incubated at 37 °C at a controlled 5% CO_2 for the time necessary to evaluate the release. Upon incubation, the medium was removed and the cells were washed in PBS, fixed with 4% paraformaldehyde (PFA), and were incubated at room temperature for 30 min. Then, MCF-7 cells were washed with PBS and treated with 0.05% triton (Invitrogen) for 5 minutes at room temperature for assuring permeability. Cells were stained with 100 μl DAPI (4′, 6-Diamidino-2-phenylindole, Sigma Aldrich) for 10 min at 4 °C in the dark. The DAPI solution was then removed and samples were washed with PBS. The initial number of cells n_{tot} deposited in each well was approximately n_{tot}~10^5.

2.7 Imaging adhering cells on the substrates. Cell adhesion o on the porous substrates was verified using an inverted Leica TCS-SP2® laser scanning confocal microscopy system equipped with an ArUv

laser, similarly to other reported experiments [22]. The pinhole and laser power were adjusted as $\sim 80 \mu m$ and 80% power respectively throughout the whole duration of the experiments. The nuclei of the cells, earlier stained with DAPI which yields blue fluorescence, were imaged on setting the laser excitation line at $405\ nm$. We acquired the images using a $10 \times$ dry objective, which permitted to work on a region of interest (ROI) $882 \times 882\ \mu m^2$ (pixel dimension $\sim 1.72\ \mu m$) in size. The described ROI is sufficiently large to contain a high number of cells, that in turn assures statistical significance. Images were averaged over at least 4 lines and 10 frames to reduce noise.

3 Results

Two different topologies of porous silicon were obtained, (i) MeP silicon, with an average pore size S smaller than 50 nm and (ii) MaP silicon, with an average pore size larger than 50 nm. The topography of MeP silicon was further adjusted to obtain substrates with a pore size in the low MeP regime, that are small pore (SP) MeP surfaces, and substrates with a pore size in the intermediate MeP regime, that are large pore (LP) MeP surfaces. Several SEM micrographs of the porous substrates were taken over different samples to assess uniformity and reproducibility. Fig.1 reproduce SEM micrographs of SP MeP, LP MeP and MaP Si surfaces taken at high $100\ K$ magnifications. These and other similar SEM images describe the morphology of the porous surfaces at the smaller scales and were elaborated [2] to derive the pore size distributions reported as the average plus or minus the standard deviation for all the analysed distributions. In doing so, we found that $S = 8 \pm 3\ nm$ for the SP MeP architecture, $S = 20 \pm 4\ nm$ for the LP MeP configuration, and $S = 55 \pm 9\ nm$ for the MaP substrates. The topography of the porous matrices was further verified through AFM imaging as in Fig.2. Fig.2a is the 3d profile of a porous surface reconstructed from AFM imaging and reported in the figure for a LP MeP substrate as an example. Fig.2b is the power spectrum derived from the 3d profile as in Fig.2a. The power spectrum delivers the information content of a surface (see Materials and Methods) and can be used to derive the fractal dimension of that surface. Using algorithms described in [20], the effective fractal dimensionality D_f of the substrates was derived, ranging from $D_f \sim 2.8$ for the substrates in the low MeP regime, to $D_f \sim 2.6$ for the intermediate MeP regime, to $D_f \sim 2.7$ for the MaP structures.

The porous substrates were loaded with the $PtCl(O,O'-acac)(DMSO)$ antitumor drug and its release verified over time. Figure 3 shows the release profile for different porous substrates reported as a fraction of the initial load. From this, one may observe that the time-dependent characteristic of the system resembles that predicted by pure diffusion (that is, a Fickian profile) for all the considered substrates, where the rate of release is high at the initial time of delivery and then it smoothly declines over time. Moreover, the total fraction of drug delivered by the porous substrates is high for the MaP architecture (~0.7) and decreases moving from MaP Si to LP MeP Si (~0.3), to SP MeP Si (~0.2). The dependency of the efficacy of delivery on pore size may be easily explained considering that larger pores may accommodate more efficiently molecules in a solution, which would then be discharged in the domain with no or minor geometrical constraints. For all the considered cases, the time constant (the time which is required by the system to reach 90% of the steady-state) falls between day 3 and day 5, that is, the porous matrix delivers its payback of therapeutics continuously for approximately 100 h. The simultaneous effects of a controlled dosage of drug and surface topography were investigated on different porous substrates as described below.

The fractal dimension is reported for all the considered substrates as a function of pore preparation in Fig.5a for ease of visualization. In Fig.5b, we report the total amount of drug released from the systems at 48 h. In agreement with the diagram of Figure 3, the drug delivered from the substrate depends on substrate preparation and pore size. Also notice that, differently from fractal dimension (Fig.5a), the released drug is a monotonic function of pore size. In Fig.5c, we report the sensitivity of MCF-7 cells to increasing concentrations of the $PtCl(O,O'-acac)(DMSO)$ antitumor drug: viable cell number was determined at a concentration of $0, 3, 6, 12\ \mu M$ 48 h after exposure and is reported in Fig.5c as a percentage of control. The reported concentrations are the equivalent of drug released from the porous substrates at different pore sizes, that are, flat Si, SP MeP, LP MeP, and MaP, as in Fig.5b. Viable cell number was determined using MTT assay following the methods reported in[23]. Values reported in Fig.5c indicate the effect of therapeutics on cell viability without the interaction with the substrate. For these, cell number is maximum (100%) when cells are treated with vanishingly small quantities of therapeutics (flat Si), then declines to 20% for a concentration of drug of $12\ \mu M$ (MaP).

Then, cell adhesion was verified on the porous substrates with and without the administration of drugs 48 h post culture. Cells were stained as described in the methods and cell images, reported

in Figure 4 for the SP MeP architecture solely, were acquired on all the porous substrates and compared to those cultured on flat silicon used as a control. Results are recapitulated in Fig.5d. Let's analyse the substrates separately. For the flat Silicon substrate, the number of cells on a substrate is on average 50. For the SP MeP architecture, the numbers of adhering cells with and without the administration of drug is $n_w \sim 118$ and $n_{w/o} \sim 205$, their ratio is ~ 0.57. For the LP MeP architecture we have $n_w \sim 30$, $n_{w/o} \sim 71$, their ratio is ~ 0.43. For the MaP silicon, we have $n_w \sim 76$, $n_{w/o} \sim 168$, and the ratio is ~ 0.45. We observe that: (i) without the administration of drug, cell adhesion is accelerated on the nanostructured surfaces and the larger the fractal dimension, the larger the number of adhering cells (compare Fig.5a and d): the number of adhering cells on porous silicon is larger than that on flat silicon for all the considered substrates; (ii) differently, when drug is released by the pores, the competition between surface topography and drug release may for some configuration make cells adhere less on a nano-porous substrate compared to flat silicon: this is the case of LP MeP Si, in which a small fractal dimension and a large pore size combine; (iii) the ratio of adhering cells on porous substrates with and without drug release (that is, $n_w/n_{w/o}$) for different substrates lightly overruns cell viability determined without cell/surface interaction as in Fig.5c, still maintaining the same trend. This suggests that, in designing advanced drug delivery systems, the effect of drug delivery and surface topography may be considered separately, and the behaviour of the entire system would result from a linear combination of these effects.

Discussions and Conclusions

Scaffolds are (often artificial) bi- and three-dimensional structures which can support and guide cell adhesion, growth and proliferation, for the integration in or the substitution of tissues or organs, and the replacement or improvement of biological functions thereof. A scaffold should be engineered to either promote or impair cell adhesion and this can be accomplished by controlling the topography of the substrate (that is, the cell surface interface) and the dosage of drugs/nutrients administrated to the cells. Here, we realized porous substrates in which the pore size and fractal dimension were varied over a significant range. Depending on pore size, the release profile of a drug may be adjusted and the dosage of released therapeutics controlled. Depending on fractal dimension, cell adhesion may be accelerated or inhibited. In culturing MCF-7 breast cancer cells on the described surfaces we observed that nano-topography and a

pore size related delivery of therapeutics combine to boost or block cell adhesion. For the particular case of tumor cells and the delivery of an anti-tumor drug, substrates with a small fractal dimension and large pore size hamper cell growth. This concept may be at the base of a rational design of implantable porous devices, drug delivery systems or scaffolds with the desired characteristics.

Figure Captions

Figure 1 SEM micrographs reveal the morphology of porous silicon. Small pore Meso-Porous (SP MeP) silicon, with an average pore size of $S = 8 \pm 3\ nm$ (a); large pore Meso-Porous (LP MeP) silicon, where $S = 20 \pm 4\ nm$ (b); and Macro-Porous silicon, with $S = 55 \pm 9\ nm$ (c).

Figure 2 Atomic force microscopy (AFM) images were acquired for all the considered cases (a) and used to de-convolve the characteristic Power Spectrum function (b): the Power Spectrum in a bi logarithmic diagram is linear and its slope is relate to the fractal dimension of the substrates.

Figure 3 Release profile of the $PtCl(O,O'-acac)(DMSO)$ antitumor drug over 350 h. The total amount of drug released and the efficiency of delivery is proportional to the pores size and smoothly increases passing from the SP MeP to the MaP architecture.

Figure 4 The nuclei of the MFC-7 breast cancer cells over flat silicon (a), SP MeP substrate without (b) and with (c) the administration of the anti-tumour drug 48 h post culture.

Figure 5 Fractal dimension reported for all the considered substrates as a function of pore preparation (a). Amount of drug released from the systems at 48 h (b). Sensitivity of MCF-7 cells to increasing concentrations of the $PtCl(O,O'-acac)(DMSO)$ antitumor drug: viable cell number was determined at a concentration of $0, 3, 6, 12\ \mu M$ (c). Number of adhering cells on all the considered substrates, with and without the administration of the anti-tumour drug, 48 h post post culture. The completion between nano-topography and drug delivery modulates cells growths and attachment on the substrates (d).

Acknowledgments

This work has been partially funded from the Italian Minister of Health (Project n. GR-2010-2320665).

References

[1] F. Gentile, E. Battista, A. Accardo, M. Coluccio, M. Asande, G. Perozziello, G. Das, C. Liberale, F. De Angelis, P. Candeloro, P. Decuzzi, E. Di Fabrizio, Fractal Structure Can Explain the Increased Hydrophobicity of NanoPorous Silicon Films, Microelectronic Engineering, 88 (2011) 2537-2540.

[2] F. Gentile, R.L. Rocca, G. Marinaro, A. Nicastri, A. Toma, F. Paonessa, G. Cojoc, C. Liberale, F. Benfenati, E. Di Fabrizio, P. Decuzzi, Differential Cell Adhesion on Mesoporous Silicon Substrates, ACS Applied Materials and Interfaces, 4 (2012) 2903–2911.

[3] H. Foll, M. Christophersen, J. Carstensen, G. Hasse, Formation and application of porous silicon, Materials Science and Engineering, 39 (2002) 93–141.

[4] Y. Hu, A. Bouamrani, E. Tasciotti, L. Li, X. Liu, M. Ferrari, Tailoring of the Nanotexture of Mesoporous Silica Films and Their Functionalized Derivatives for Selectively Harvesting Low Molecular Weight Protein, ACS Nano, 4 (2010) 439–451.

[5] H.H.P. Yiu, P.A. Wright, Enzymes Supported on Ordered Mesoporous Solids: a Special Case of an Inorganic-Organic Hybrid, Journal of Materials Chemistry, 15 (2005) 3690–3700.

[6] S. Godefroo, M. Hayne, M. Jivanescu, A. Stesmans, M. Zacharias, O.I. Lebedev, G.V. Tendeloo, V.V. Moschalkov, Classification and control of the origin of photoluminescence from Si nanocrystals, Nature Nanotechnology, 3 (2008) 174-178.

[7] C. Cosentino, F. Amato, R. Walczak, A. Boiarski, M. Ferrari, Dynamic Model of Biomolecular Diffusion through Two-Dimensional Nanochannels, Journal of Physical Chemistry B, 109 (2005) 7358-7364.

[8] S.L. Tao, T.A. Desai, Microfabricated drug delivery systems: from particles to pores, Advanced Drug Delivery Reviews, 55 (2003) 315–328.

[9] J.S. Ananta, B. Godin, R. Sethi, L. Moriggi, X. Liu, R.E. Serda, R. Krishnamurthy, R. Muthupillai, B.R. D, L. Helm, M. Ferrari, L.J. Wilson, P. Decuzzi, Geometrical confinement of gadolinium-based contrast agents in nanoporous particles enhances T1 contrast, Nature Nanotechnology, 5 (2010) 815-821.

[10] M. Gaspari, M.M.-C. Cheng, R. Terracciano, X. Liu, J. Nijdam, L. Vaccari, E. Di Fabrizio, E.F. Petricoin, L.A. Liotta, G. Cuda, S. Venuta, M. Ferrari, Nanoporous surfaces as harvesting agents for mass spectrometric analysis of peptides in human plasma, Journal of Proteome Research, 5 (2006) 1261-1266.

[11] F. Gentile, A. Accardo, M. Coluccio, M. Asande, G. Cojoc, F. Mecarini, G. Das, C. Liberale, F. De Angelis, P. Candeloro, P. Decuzzi, E. Di Fabrizio, NanoPorous- MicroPatterned-SuperHydrophobic Surfaces as Harvesting Agents For Low Molecolar Weight Molecules, Microelectronic Engineering, 88 (2011) 1749-1752.

[12] F. Gentile, M. Coluccio, A. Accardo, G. Marinaro, E. Rondanina, S. Santoriello, S. Marras, G. Das, L. Tirinato, G. Perozziello, F. De Angelis, C. Dorigoni, P. Candeloro, E. Di Fabrizio, Tailored Ag nanoparticles/nanoporous superhydrophobic surfaces hybrid devices for the detection of single molecule, Microelectronic Engineering, 97 (2012) 349–352.

[13] F. Gentile, M.L. Coluccio, R.P. Zaccaria, M. Francardi, G. Cojoc, G. Perozziello, R. Raimondo, P. Candeloroa, E.D. Fabrizio, Selective on site separation and detection of molecules in diluted solutions with superhydrophobic clusters of plasmonic nanoparticles, Nanoscale, 6 (2014) 8208-8225.

[14] R. Terracciano, M. Gaspari, F. Testa, L. Pasqua, P. Tagliaferri, M.M.-C. Cheng, J. Nijdam, E.F. Petricoin, L.A. Liotta, G. Cuda, M. Ferrari, S. Venuta, Selective binding and enrichment for low-molecular weight biomarker molecules in human plasma after exposure to nanoporous silica particles, Proteomics, 6 (2006) 3243-3250.

[15] J. Clarke, H.-C. Wu, L. Jayasinghe, A. Patel, S. Reid, H. Bayley, Continuous base identification for single-molecule nanopore DNA sequencing, Nature Nanotechnology, 4 (2009) 265-270.

[16] Y. Astier, L. Data, R.P. Carney, F. Stellacci, F. Gentile, E. Di Fabrizio, Artificial Surface-Modified Si3N4 Nanopores for Single Surface-Modified Gold Nanoparticle Scanning, Small, 7 (2010) 455-459.

[17] Y.L. Khung, G. Barritt, N.H. Voelcker, Using continuous porous silicon gradients to study the influence of surface topography on the behaviour of neuroblastoma cells, Experimental Cell Research, 314 (2008) 789–800.

[18] G. Marinaro, R. La Rocca, A. Toma, M. Barberio, L. Cancedda, E. Di Fabrizio, P. Decuzzi, F. Gentile, Networks of Neuroblastoma Cells on Porous Silicon Substrates Reveal a Small World Topology, Integrative Biology, 7 (2015) 184-197.

[19] F. Gentile, M. Coluccio, A. Toma, E. Rondanina, M. Leoncini, F. De Angelis, G. Das, C. Dorigoni, P. Candeloro, E. Di Fabrizio, Electroless deposition dynamics of silver nanoparticles clusters: A diffusion limited aggregation (DLA) approach Microelectronic Engineering, 98 (2012) 359-362.

[20] F. Gentile, L. Tirinato, E. Battista, F. Causa, C. Liberale, E. Di Fabrizio, P. Decuzzi, Cells preferentially grow on rough substrates, Biomaterials, 31 (2010) 7205-7212.

[21] A. Muscella, C. Vetrugno, D. Migoni, F. Biagioni, F.P. Fanizzi, F. Fornai, S.A. De Pascali, S. Marsigliante, Antitumor activity of [Pt(O,O'-acac)(γ-acac)(DMS)] in mouse xenograft model of breast cancer, Cell Death Diseases, 5 (2014) e1014.

[22] P. Decuzzi, F. Gentile, A. Granaldi, A. Curcio, F. Causa, C. Indolfi, P. Netti, F. M, Flow chamber analysis of size effects in the adhesion of spherical particles, International Journal of Nanomedicine, 2 (2007) 689–696.

[23] A. Muscella, N. Calabriso, F. Fanizzi, S. De Pascali, L. Urso, A. Ciccarese, D. Migoni, S. Marsigliante, [Pt(O,O0-acac)(c-acac)(DMS)], a new Pt compound exerting fast cytotoxicity in MCF-7 breast cancer cells via the mitochondrial apoptotic pathway, British Journal of Pharmacology, 153 (2008) 34–49.

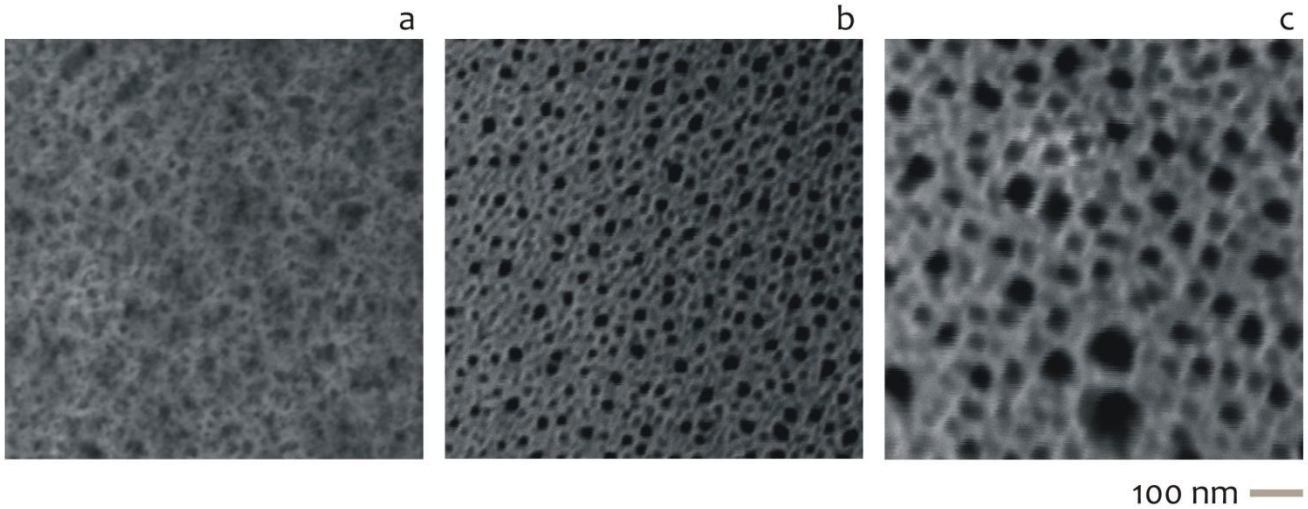

Fig. 1

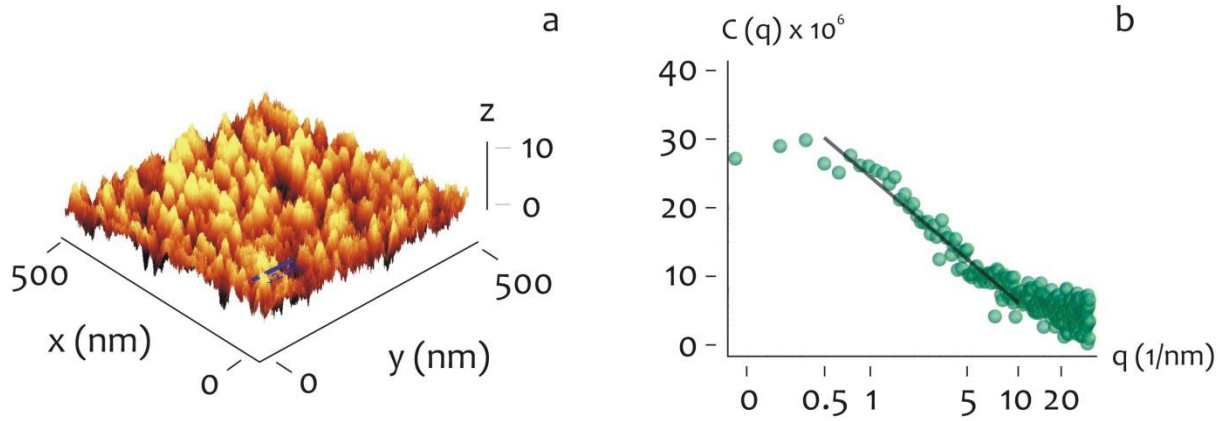

Fig. 2

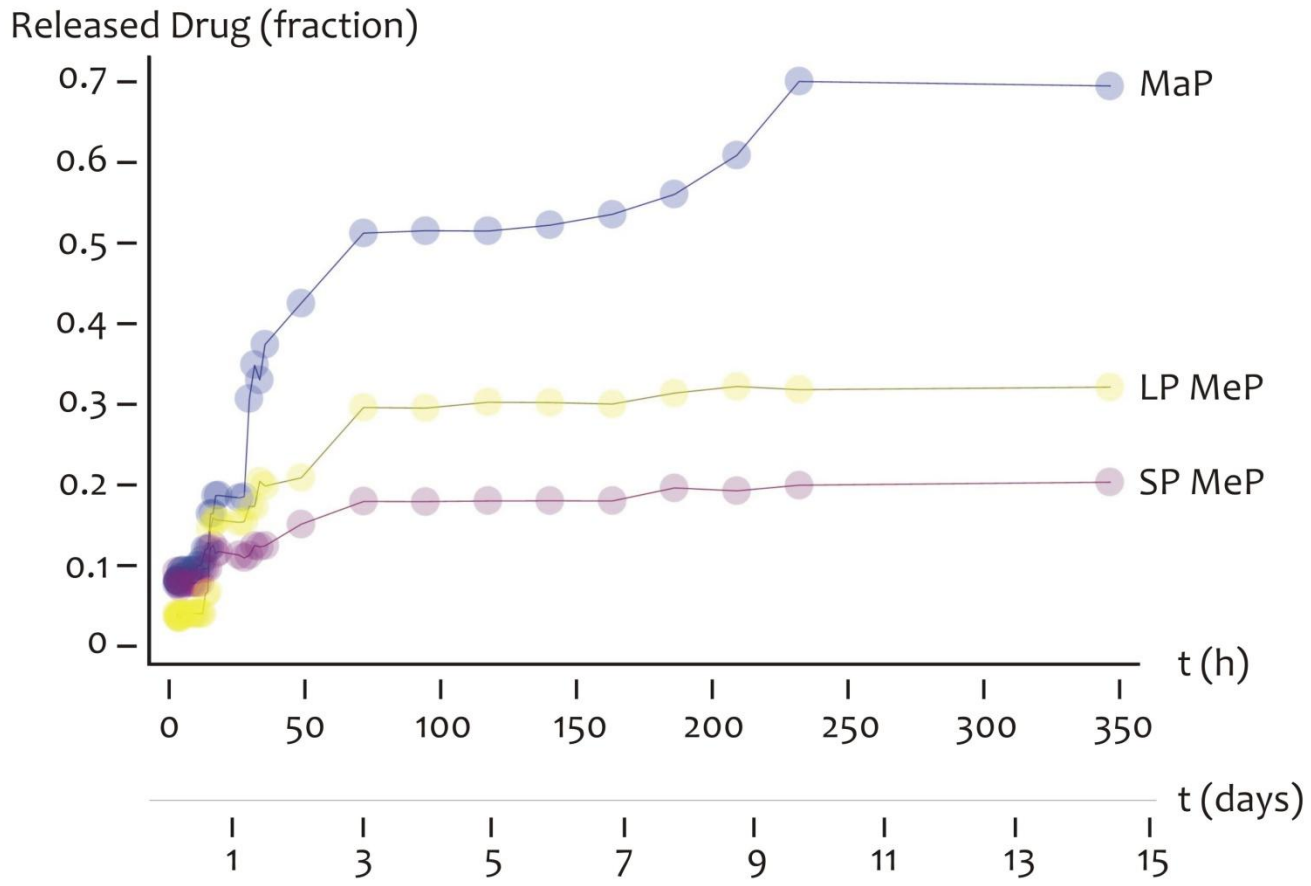

Fig. 3

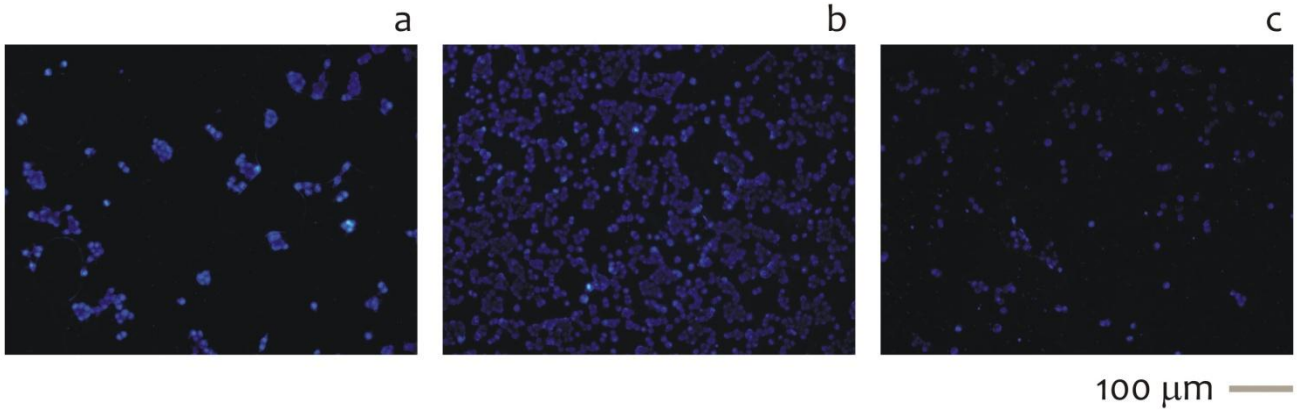

Fig. 4

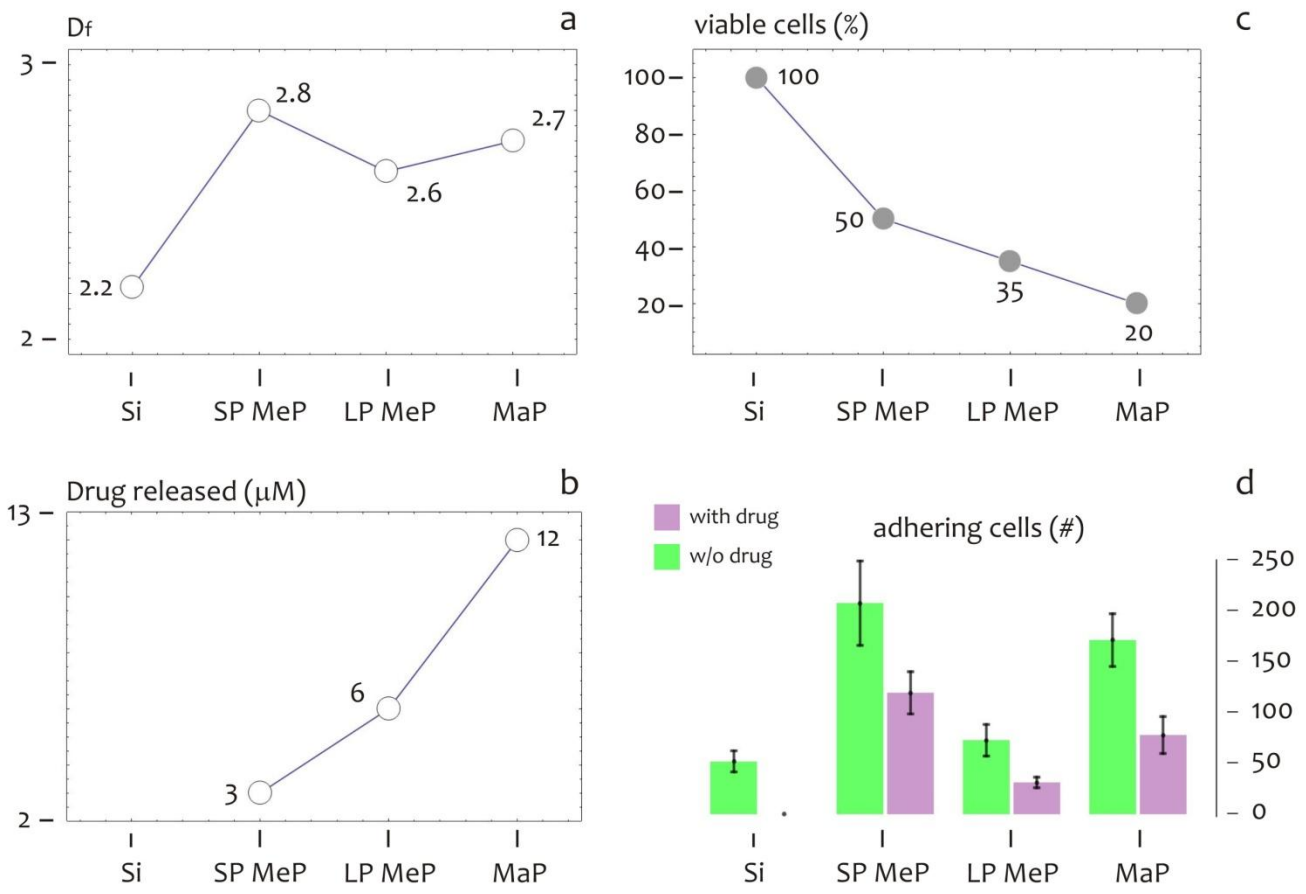

Fig. 5

Graphical abstract

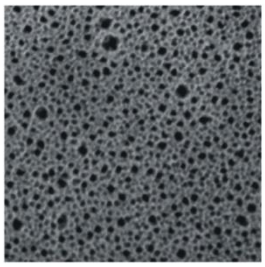

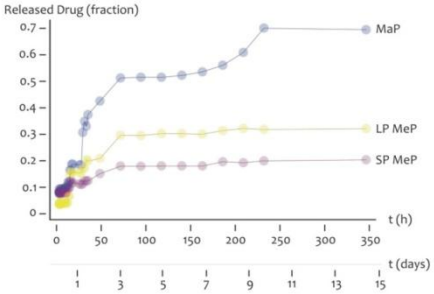

Highlights

- We realized porous silicon substrates with a varying pore size and fractal dimension
- We loaded the substrates with an antitumor drug and determined its release profile over time
- We verified the adhesion of MCF-7 cancer cells on the porous substrates
- We decoupled the effects of nano-topography and drug delivery on cell adhesion
- Large pore sizes boost drug release, large fractal dimensions accelerate cell adhesion